Journal of Magnetism and Magnetic Materials 475 (2019) 602–610

Contents lists available at ScienceDirect

Journal of Magnetism and Magnetic Materials

journal homepage: www.elsevier.com/locate/jmmm

Research articles

Metalloporphyrins-sensitized titania-silica-iron oxide nanocomposites with high photocatalytic and bactericidal activities under visible light irradiation

Padtaraporn Chanhom[a], Nisanart Charoenlap[b], Chonnavee Manipuntee[a], Numpon Insin[a,*]

[a] Department of Chemistry, Faculty of Science, Chulalongkorn University, Bangkok 10330, Thailand
[b] Laboratory of Biotechnology, Chulabhorn Research Institute, Bangkok 10210, Thailand

ARTICLE INFO

Keywords:
Photocatalyst
Nanocomposite
Magnetic
Titania
Metalloporphyrin

ABSTRACT

Multifunctional photocatalyst system of meso-tetra(4-carboxyphenyl)porphyrin (TCPP) with different metal centers [Mn(II), Fe(III), Cu(II), Zn(II) and metal-free] adsorbed on titania-silica-iron oxide magnetic photocatalyst nanocomposites (TSI) that united superparamagnetic behavior and high photoactive activity under visible light irradiation have been prepared. The superparamagnetic nanocomposites have been characterized and analyzed using UV-visible absorption spectroscopy, X-ray diffractometry (XRD), transmission electron microscopy (TEM), Fourier transform infrared spectroscopy (FT-IR), and X-ray photoelectron spectroscopy (XPS). The results showed that copper(II)tetra(4-carboxyphenyl)porphyrin -sensitized titania-silica-iron oxide nanocomposites (CuTCPP-TSI) can effectively degrade methylene blue (MB) and kill *Escherichia coli* (*E. coli*) under irradiation with an incandescent lamp. The magnetic photocatalysts could be used at least four times without regeneration. Therefore, the CuTCPP-TSI nanocomposites can be applied in catalytic photodegradation and used for magnetically-guided antibacterial applications.

1. Introduction

Titania (titanium dioxide) has been the most widely used photocatalyst due to its various superior properties such as high photocatalytic activity under ultraviolet (UV) region, high chemical stability, low toxicity and environmental friendliness [1]. However, the titania nanoparticles need to be activated by the UV irradiation to excite the titania nanoparticles to photoactive materials. Unfortunately, only a very small fraction (4–6%) of the solar spectrum is in UV region, whereas 45% of the solar spectrum falls in visible region [2]. Thus, there is a motivation to develop an efficient visible light-responsive photocatalysts to extend their spectral response to longer absorption wavelength. Titania nanoparticles can be modified using various methods [2] such as metals doping, non-metal doping, and surface sensitization by organic dyes. Among these methods, the sensitization method can effectively extend the range of visible light absorption.

Porphyrins are organic dyes with high chemical stability in comparison to other dyes, and their redox properties can be easily tuned using metal complexation [3]. Metallopophyrins are considered as efficient sensitizers to harvest light on the surface of titania. Because of an extensive system of delocalized π electrons, porphyrins exhibit very strong absorption in the visible light. The sensitization of titania nanoparticles by porphyrins is also considered as an effective approach to improve visible spectral absorption and photocatalytic degradation of organic pollutants such as methylene blue [4], luminol [5] and atrazine [6] under visible irradiation as previously reported.

Other than photodegradation of organic pollutants, photocatalysis is an efficient technology to eliminate bacteria from aquatic environment. Titania particles have been examined as efficient alternatives to inactivate a variety of harmful bacteria [7]. When titania photocatalysts are illuminated with UV irradiation, TiO_2 achieves strong oxidizing power and can generate reductive oxygen species (ROS) such as $OH^{\cdot}$ and $O_2^{\cdot -}$. Some studies have confirmed that these ROS could destroy the outer membrane of the *Escherichia coli* (*E. coli*) cell, and finally the cell itself [7,8]. Recently, advances in bacterial disinfection using visible light activated-titania photocatalytic materials are also reviewed here. A 5%Cu-doped TiO_2/glass fibers was used for the disinfection of *E. coli* in bioaerosols under visible light irradiation [9]. Under a moderate level of humidity, the highest disinfection efficiency of *E. coli* was reported as 87.8%. For another study, Zargari *et al.* produced TiO_2-3%graphene nanocomposite sensitized with SnTCPP and investigated that more than 99% of the *E. coli* cells were killed within 260 min under the visible light irradiation [10].

However, the use of titania slurry is still limited mainly because it is difficult to separate and recover these nanoparticles from the liquid phase [1,11]. In order to solve the separation problem, some researchers prepared composite photocatalysts with magnetic nanoparticle cores and titania shells [11]. In our previous study [12], we found that the titania-coated magnetic microspheres showed lower photoactivity than the titania-silica-

* Corresponding author.
E-mail address: Numpon.I@chula.ac.th (N. Insin).

https://doi.org/10.1016/j.jmmm.2018.11.090
Received 24 June 2018; Received in revised form 8 November 2018; Accepted 18 November 2018
Available online 19 November 2018
0304-8853/

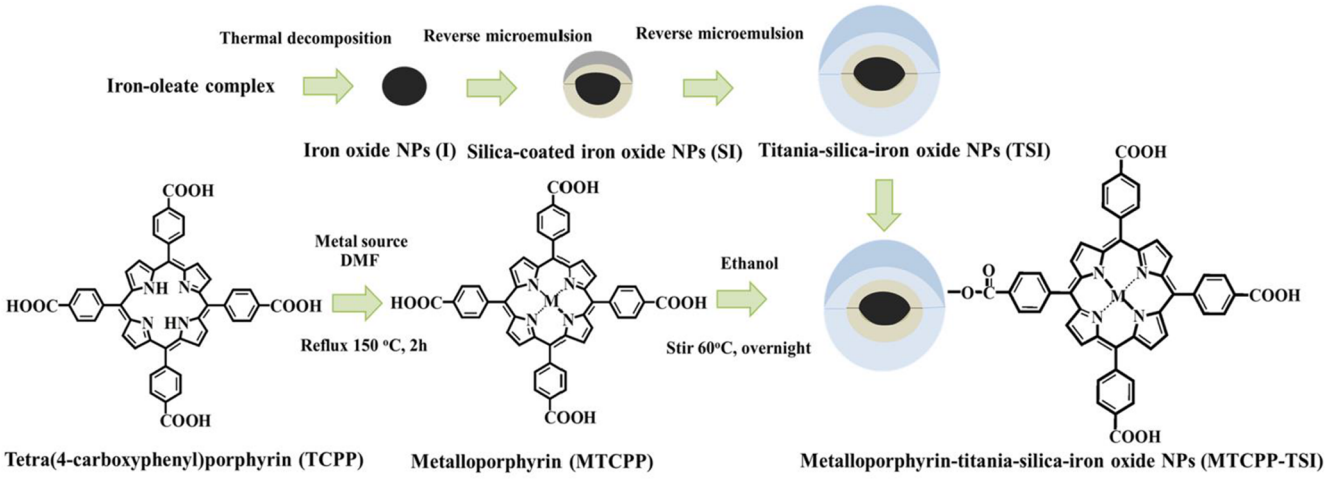

Fig. 1. Scheme for the synthesis of metalloporphyrin-sensitized titania-silica-iron oxide nanocomposites.

iron oxide (TSI) nanocomposites due to the enhanced rate of recombination of electron and hole when iron oxide was in direct contact with titania as iron oxide core becomes the recombination center of photogenerated electrons and holes. We observed that the amorphous silica interlayer could prevent the direct electrical contact between the magnetic core and the titania shell, and thus increase the photocatalytic activity of the composite photocatalyst.

In this research, we demonstrate the procedures for preparing visible light-active photocatalysts with superparamagnetic character by attaching TCPP with different metal centers onto TSI nanocomposites. It has been studied that TCPP can be especially strongly adsorbed onto the surface of titania nanoparticles under stirring at 60 °C overnight [6]. The photocatalytic activities of the nanocomposites were then investigated by measuring the degradation of methylene blue solution upon visible light irradiation compared with bare TSI nanocomposites. The effects of metal center of TCPP on the photocatalytic efficiency were studied, and the optimal condition for the photodegradation of methylene blue was obtained. Finally, bactericidal activity of these nanocomposites against *E. coli* under visible light was tested to demonstrate the applications in visible light disinfection using the magnetically removable photocatalyst.

2. Experimental section

2.1. Materials

Iron (III) chloride hexahydrate ($FeCl_3{\cdot}6H_2O$), 1-octadecene, Igepal CO-520, Tetrabutyl orthotitanate (TBOT), Tetra(4-carboxyphenyl)porphyrin (TCPP), N,N'-dimethylformamide (C_3H_7NO, DMF) were purchased from Aldrich. Tetraethyl orthosilicate (TEOS) and cetyltrimethylammonium bromide ($C_{19}H_{42}BrN$, CTAB) were purchased from Fluka. All chemical reagents were analytical grade.

2.2. Synthesis of magnetic nanocomposites

Syntheses of titania-silica-iron oxide nanoparticles were performed according to our previous work [12]. Briefly, iron oxide nanoparticles were firstly prepared using $FeCl_3{\cdot}6H_2O$ and oleic acid as the main precursors for iron-oleate complex. Then, the complex was thermally decomposed at 320 °C for 30 min under nitrogen flow, and the iron oxide nanoparticles were precipitated using ethanol [13]. The silica-coated iron oxide nanoparticles were prepared by the reverse microemulsion method using 600 μL of tetraethyl orthosilicate (TEOS) as silicon source. In a typical synthesis, Igepal CO-520 was dispersed in cyclohexane, and then iron oxide nanoparticles were added to the solution. Ammonium hydroxide solution was used as a catalyst. The reaction was stirred for 16 h at room temperature. The product was collected by centrifugation and washed with ethanol. The coating of titania on the iron oxide/silica surface to obtain titania-silica-iron oxide nanocomposites was done according to the following procedure. Hexanol, cetyltrimethylammonium bromide (CTAB) and water were formed into micelles in hexanol, before tetrabutyl orthotitanate (TBOT) was added into the solution. The reaction mixture was refluxed at 80 °C for 24 h. After refluxed, the sample was collected by centrifugation and washed with DI water and ethanol.

Metalloporphyrins (MTCPPs) were prepared by refluxing TCPP with metal sources (copper(II) chloride dihydrate, zinc(II) acetate dihydrate, iron(III) chloride, manganese(II) acetate) in dimethylformamide (DMF) at 150 °C for 2 h. DMF was removed, and MTCPPs were precipitated by adding water. The precipitate was dissolved in NaOH solution and re-precipitated by adding HCl solution. MTCPP were obtained after dissolved in ethanol and evaporated [6].

In order to form MTCPP-TSI nanocomposites, metalloporphyrin complexes were dissolved in ethanol solution, and then titania-silica-iron oxide nanocomposites were added into the solution. The mixture was continuously stirred overnight at 60 °C. The products metalloporphyrin-sensitized titania-silica-iron oxide nanocomposites (MTCPP-TSI) were collected using centrifugation and washed with ethanol. Overall process for the preparation of the magnetic nanocomposites is shown in Fig. 1.

2.3. Characterization methods

X-ray Electron Diffraction (XRD) characterization was performed using a D/MAX 2200 X-ray diffractometer (Rigaku, Japan) with Cu-Kα radiation at an accelerating voltage of 40 kV and an applied current of 30 mA. The XRD patterns of the composites, iron oxides and titania nanoparticles were recorded at 2θ in a range of 20°–70°. TEM images were taken using a JEOL 2100 microscope (Japan) operated at 120 kV. One drop of the colloidal solutions, prepared by dispersing a small amount of nanoparticles in ethanol using an ultrasonic treatment for at least 2 min, was placed onto a Formvar-coated copper grid and dried at room temperature for TEM measurement. The images were used to study the sizes and morphology of particles and the thickness of the coating of the layers. The selected area electron diffraction pattern was taken by a Hitachi transmission electron microscope (HT7700). Absorption spectra of solutions were measured on a HP 8453 (Agilent, USA) UV-vis spectrophotometer. A Malvern Zetasizer Nano ZSP was used to measure the hydrodynamic size distribution of the nanocomposites. The X-ray photoelectron spectrometer (XPS) was performed by PHI5000 Versa Probe II (ULVAC-PHI, Japan) using monochromated Al Kα radiation, and the binding energies were corrected using adventitious carbon (C1s at 284.6 eV). The Fourier transform infrared spectrometry (FT-IR) performed using a Nicolet 6700 FT-IR spectrometer operating in transmission mode was used to confirm the functional groups on all samples. The transmission spectra were obtained after a mixture of sample and KBr

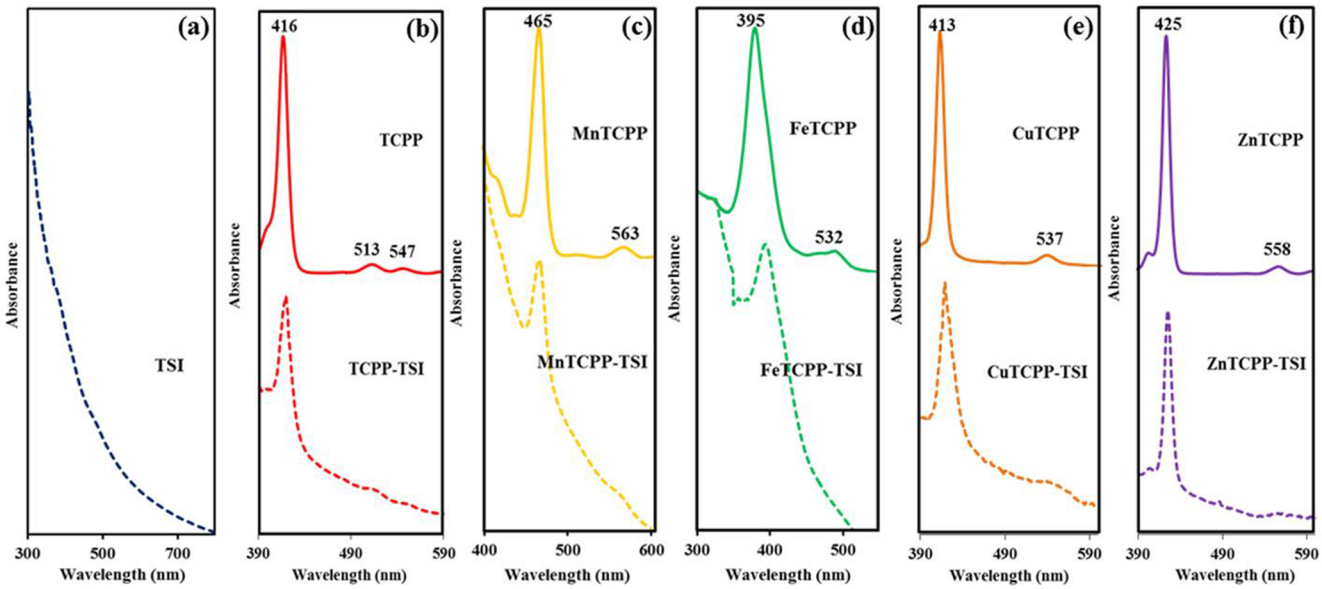

Fig. 2. UV-Vis absorption spectra of (a) TSI, (b) TCPP and TCPP-TSI, (c) MnTCPP and MnTCPP-TSI, (d) FeTCPP and FeTCPP-TSI, (e) CuTCPP and CuTCPP-TSI, and (f) ZnTCPP and ZnTCPP-TSI nanocomposites.

powder was pressed into a pellet. The magnetization of samples was carried out at room temperature using a vibrating sample magnetometer (Lakeshore model 730908, USA).

2.4. Photocatalytic degradation measurement

The photocatalytic activity of the synthesized nanocomposites was investigated by measuring the degradation of methylene blue solution upon visible light irradiation and compared with the TSI nanoparticles. A 100 W incandescent lamp is used as the visible irradiation light source. For each photocatalytic experiment, 10 mg of photocatalyst nanoparticles is dispersed in a 30 mL aqueous solution of 7 ppm methylene blue. The suspension was kept in a dark chamber for 1 h to obtain an adsorption-desorption equilibrium among the catalyst, water and the dye before irradiation. At given intervals of visible light irradiation, samples were collected after the catalyst was separated from the solution using a magnet. The photocatalytic ability of the MTCPP-TSI nanocomposites was compared with the TSI nanocomposites by determining the photodegradation of methylene blue measured by the decrease of the dye absorbance at 664 nm.

The reusability of the catalyst was investigated by repeating the photocatalytic cycles of the selected MTCPP-TSI showing the highest efficiency. The reused catalyst experiment was done according to the measurement of photocatalytic activity mentioned earlier. The catalyst was collected from methylene blue solution using a magnet. The photocatalytic cycle was repeated for four times. Various concentrations of methylene blue ranging from 5 ppm to 15 ppm (5 ppm, 7 ppm, 10 ppm, 15 ppm) were used to determine photocatalytic activity for degradation of 30 mL methylene blue solution under visible light irradiation (3 h), while the amount of photocatalysts was kept constant at 10 mg for each testing.

2.5. Antibacterial activity

The bacteria killing assay was performed as previous described with slight modification [12]. Culture of *E. coli* cells were grown aerobically in 5 mL Luria-Bertani (LB) broth at 37 °C with 150 rpm shaking for overnight. The bacterial cells were sub-cultured into a fresh LB broth and grown until reaching an optical density at 600 nm of 0.5. The exponential phase cells were harvested by centrifugation at 7000 rpm for 10 min and then resuspended in sterilized normal saline (0.9% sodium chloride). The bacterial suspensions were treated with CuTCPP-TSI magnetic nanocomposites illuminated by a 100 W incandescent lamp at 37 °C for 3 h. After irradiation, survival cells were enumerated by viable cell count method. The colony-forming units (CFU) were scored after incubation at 37 °C for overnight. The cells treated with light alone were used as a control experiment and conducted in parallel.

3. Results and discussion

The metalation of porphyrin was determined by UV-vis spectroscopy. The UV-vis absorption band maxima of metal-free porphyrin (TCPP) and metalloporphyrins (MTCPPs) are compared in Fig. 2. For metal-free porphyrin (TCPP) in ethanol, the strong Soret band appears at 416 nm, and four Q bands are at 513, 547, 591, 644 nm. The Soret band and Q band are caused by the electron transition of $a_{1u}(\pi)$–$e_g^*(\pi)$ and $a_{2u}(\pi)$–$e_g^*(\pi)$ of porphyrin structure, respectively [14]. The Soret band of TCPP was shifted to a higher or shorter wavelength depending on metals in the porphyrin. Compared to metal-free porphyrin (TCPP), the absorption bands of CuTCPP and FeTCPP present a blue shift. However, comparison between metal-free porphyrin (TCPP), MnTCPP and ZnTCPP, the absorption bands of MnTCPP and ZnTCPP present a red shift, which agrees well with the previous report [6]. The insertion of different transition metals into the TCPP (free-base porphyrin) causes changes to the absorption features both intensity and wavelength [14]. The red shifted Soret absorption bands were observed in the out-of-plane metalloporphyrins as Mn^{2+} and Zn^{2+} are borderline metalloporphyrins. In contrast, the blue shifted UV–Vis absorption bands are presented in the in-plane metalloporphyrins such as Fe^{3+} and Cu^{2+} substituents in porphyrin. Because the positions of Fe^{3+} and Cu^{2+} are fixed within the cavity of the porphyrin ligand, the atomic orbitals of the metal centers are able to overlap more strongly with the highest occupied molecular orbitals (HOMO) of the ligand, resulting in the reduction in the energy level of HOMO without the change in level of the lowest unoccupied molecular orbitals (LUMO). Therefore, the energy gaps of the ligand in FeTCPP and CuTCPP increase as observed as the decrease in the absorption wavelengths. On the contrary, for the out-of-plane metalloporphyrins, the atomic orbitals of the metal centers bounded weakly with the HOMO but have more interaction with LUMO. The unchanged HOMO and lower LUMO energy level leads to an increase in the wavelengths [15].

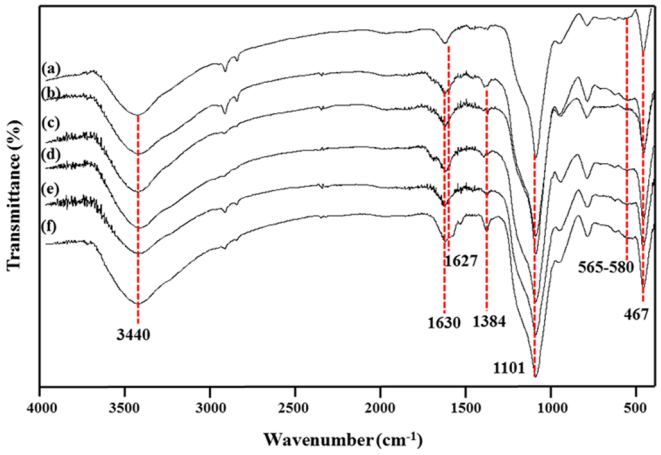

Fig. 3. FT-IR spectra of (a) titania-silica-iron oxide nanocomposites (TSI), (b) TCPP-TSI nanocomposites, (c) MnTCPP-TSI nanocomposites, (d) FeTCPP-TSI nanocomposites, (e) CuTCPP-TSI nanocomposites, (f) ZnTCPP-TSI nanocomposites.

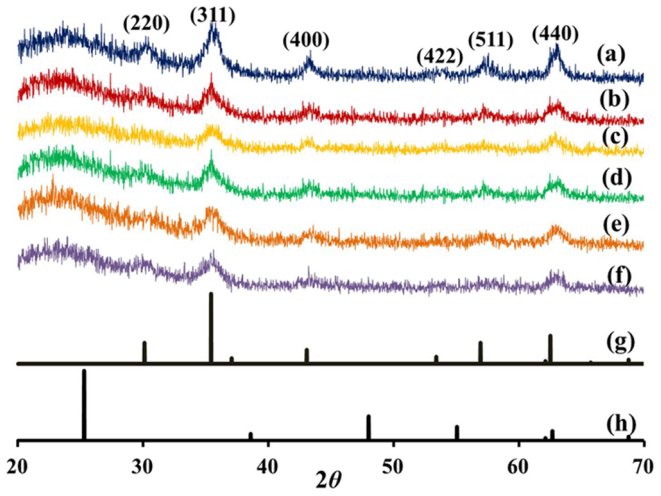

Fig. 4. X-ray diffraction patterns of (a) TSI nanocomposites, (b) TCPP-TSI nanocomposites, (c) MnTCPP-TSI nanocomposites, (d) FeTCPP-TSI nanocomposites, (e) CuTCPP-TSI nanocomposites, (f) ZnTCPP-TSI nanocomposites (g) JCPDS no. 19-0629 (magnetite phase), (h) JCPDS no. 21-1272 (anatase phase).

The absorption spectra of porphyrins adsorbed onto titania surface nanocomposites are similar to those of the corresponding free porphyrins spectra with a small red shift likely due to the interaction between TSI magnetic composites surface and the carboxylate groups of porphyrins. Metalloporphyrin-sensitized TSI nanocomposites (MTCPP-TSI) exhibited a new absorption band falling in the range of the solar spectrum better than the TSI magnetic nanocomposites. The absorption spectra of the MTCPP-TSI composites suggested that the nanocomposites can utilize visible light for photocatalytic application.

To better understand the interaction between TSI and MTCPPs, IR spectroscopy was used in the comparison between the bonds in TSI and MTCPP-TSI. In the FT-IR spectrum of TSI magnetic composites (Fig. 3a), all the prominent signals were corresponding to the bonds in titania, silica and iron oxide. The absorption band at 3440 cm^{-1} was attributed to O—H stretching of titania. The band at 1627 cm^{-1} was assigned to the bending vibration of O—H group [16]. The asymmetric Si—O—Si stretching band can be observed at 1101 cm^{-1}. The small broad band at 565–580 cm^{-1} was indicative of the stretching mode of Fe—O in iron oxide, even though it was in a low concentration. The stretching vibration peak of Ti-O-Ti band belong to titania appeared at 467 cm^{-1} [16]. As shown in Fig. 3(b–f), MTCPP-TSI nanocomposites exhibited two new peaks appearing at 1630 and 1384 cm^{-1}, which were assigned to the asymmetric (overlap with the bending vibration of O—H bond) and symmetric stretches of $-COO^{-}$ [4,16]. The observation of carboxylate group suggested that metalloporphyrin molecules were successfully chemisorbed as carboxylates on the surface of TSI magnetic composites.

The crystal structure of TSI and MTCPP-TSI were characterized by XRD as shown in Fig. 4. The MTCPP-TSI nanocomposites (Fig. 4b–d) featured mixed diffraction peaks of strong signals from magnetite (JCPDS no. 19-0629) and weaker signals from anatase titania (JCPDS no. 21-1272) [12], indicating the higher crystallinity of iron oxide phase than anatase titania, while the amorphous silica did not show any signals. After the modification with metalloporphyrins, the characteristic diffraction peaks of all composites in XRD patterns do not exhibit any shifts in peak shape, confirming that the modification has no influence on the crystal structure of TSI magnetic nanocomposites (Fig. 4a). However, no refraction peaks were observed for metalloporphyrin molecules in all XRD patterns, indicating that the metalloporphyrins did not stay as separated phases, but rather stayed as a thin layer coating on TSI. From the XRD studies, it can be confirmed that the composites can have both the ferrimagnetic character of magnetite phase and the photocatalytic property from the anatase phase. In addition, crystalline size of magnetite could be estimated from the parent peak of the (3 1 1) plane using the Debye-Scherrer equation. The

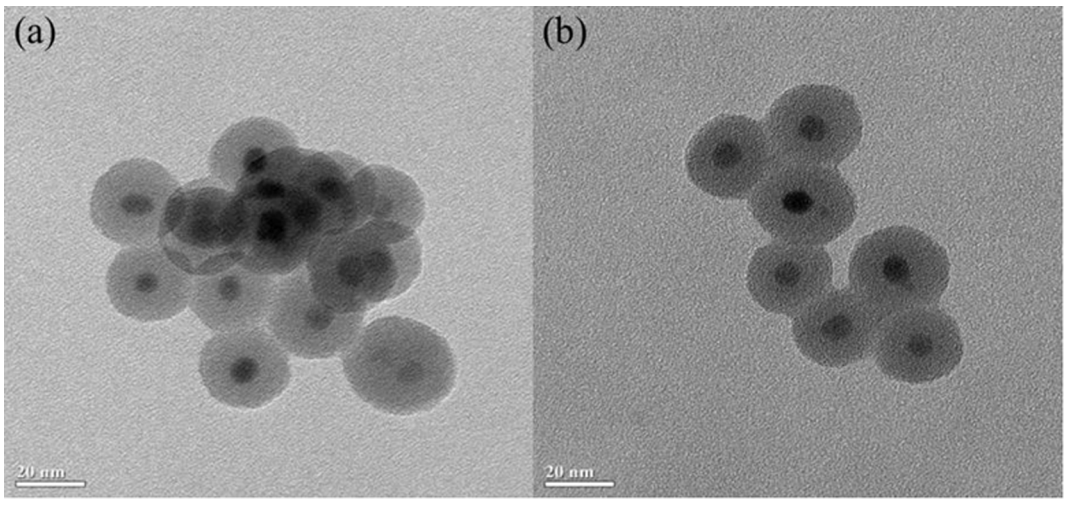

Fig. 5. The TEM images of (a) TSI and (b) CuTCPP-TSI nanocomposites.

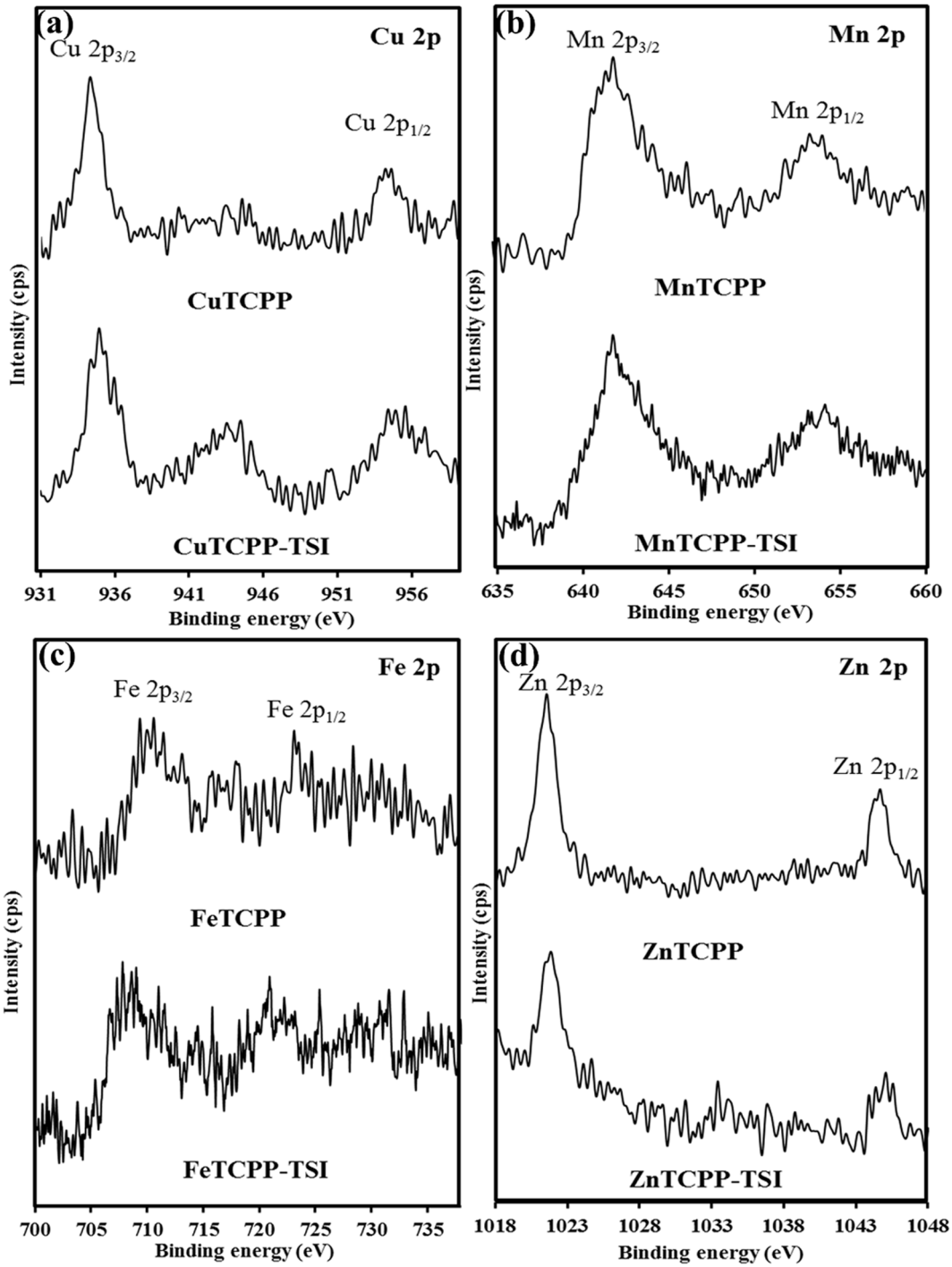

Fig. 6. High-resolution XPS spectra of (a) Cu 2p of CuTCPP and CuTCPP-TSI, (b) Mn 2p of MnTCPP and MnTCPP-TSI, (c) Fe 2p of FeTCPP and FeTCPP-TSI, and (d) Zn 2p of ZnTCPP and ZnTCPP-TSI nanocomposites.

calculated crystalline sizes of all nanocomposites were reported in Table S1 showing the size range of 5.33–6.28 nm, indicating that the preparation process and the presence of MTCPPs did not much affect the size of magnetic nanoparticles.

To observe the sizes and morphology of the nanocomposites, TEM was used in comparing TSI and a selected representative MTCPP-TSI, CuTCPP-TSI. From TEM image in Fig. 5, both nanocomposites are of similar sizes and structures. TSI nanocomposites displayed a core-shell structure with a uniform size. The dark gray iron-oxide nanoparticles (core) had a mean diameter of about 8–10 nm. Silica interlayer and titania layer (gray shell) were completely coated on the iron oxide nanoparticles as has been investigated in our previous study [12]. After the composite has undergone the surface modification with CuTCPP, CuTCPP-TSI nanoparticles displayed uniform spherical shape, with an average diameter of about 26.5 nm. Moreover, the selected area electron diffraction pattern of CuTCPP-TSI (Fig. S1 in Supplementary) exhibited the five distinct ring pattern that is characteristic of the magnetite nanocrystallites. The d-spacings matched well with the major d-spacings of magnetite phase and agreed well with the results from XRD. TEM image of CuTCPP-TSI nanoparticles indicated that these composites were of core-shell structure, which is similar to that of the TSI composites. These results demonstrated that the surface modification of

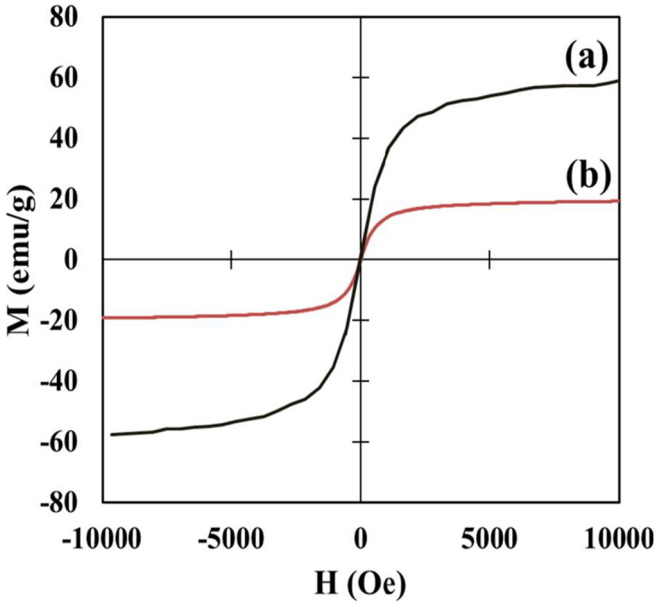

Fig. 7. Magnetization versus magnetic field curves of the (a) iron oxide (I) nanoparticles, and (b) Cu(II) porphyrin-sensitized titania-silica-iron oxide (CuTCPP-TSI) nanocomposites.

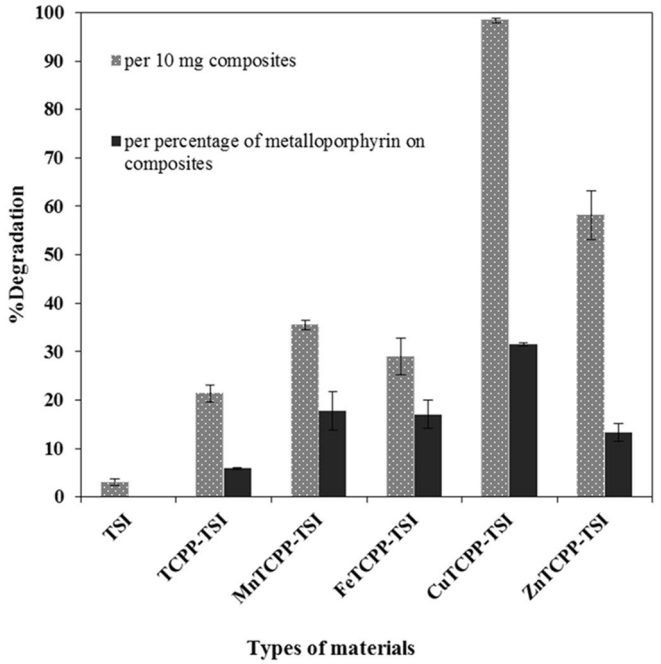

Fig. 8. Degradation of methylene blue with TSI, TCPP-TSI, MnTCPP-TSI, FeTCPP-TSI, CuTCPP-TSI, and ZnTCPP-TSI nanocomposites under visible light irradiation.

TSI with CuTCPP did not affect the structure and the aggregation of the TSI nanocomposites.

To investigate the stability of the nanocomposites when dispersed in water-based solution, hydrodynamic sizes of the nanocomposites were analyzed using a Malvern Zetasizer Nano ZSP. According to the dynamic light scattering (DLS) size measurements from Table S2 and Fig. S2 in Supplementary, the average hydrodynamic particle sizes of CuTCPP-TSI and TSI were both less than 150 nm with a small increase in the size of the nanocomposites after attached with CuTCPP. From the hydrodynamic size and size distribution of the nanocomposites, no sign of large aggregation was observed in the dispersion of the nanocomposites during the time of measurement, suggesting that the homogeneous dispersion of the nanocomposites could be obtained during the use of the nanocomposite photocatalysts.

XPS analysis was used for determining the surface chemical composition and oxidation state of transition metal ion in metalloporphyrins before and after forming the composites with TSI. The XPS spectra of different metals in MTCPPs modified on composite surface and the corresponding free metalloporphyrins were provided in Fig. 6. The high resolution XPS spectra of Cu, Mn, Fe, Zn were detected in CuTCPP and CuTCPP-TSI, MnTCPP and MnTCPP-TSI, FeTCPP and FeTCPP-TSI, ZnTCPP and ZnTCPP-TSI, respectively. The binding energies indicated the oxidation state of metals in the prepared metalloporphyrin TSI composites. For CuTCPP and CuTCPP-TSI, two separate peaks located at 934.5 and 954.4 eV were due to Cu ($2p_{3/2}$) and Cu ($2p_{1/2}$) transitions, respectively. These binding energies correspond to Cu^{2+} [9]. For MnTCPP-TSI spectra, two peaks can be found at Mn ($2p_{3/2}$) and Mn ($2p_{1/2}$), which were assigned to Mn^{2+}. For FeTCPP-TSI nanocomposites, the Fe ($2p_{3/2}$) peak and the Fe ($2p_{1/2}$) peak of FeTCPP in FeTCPP-TSI sample appeared at binding energies of 710.7 and 724.1 eV, respectively. These result indicated the existence of Fe^{3+} in FeTCPP-TSI magnetic samples. The binding energies of 1021.9 and 1045.1 eV for Zn (2p) also confirmed the oxidation state of Zn (Zn^{2+}) [17]. For all the XPS spectra, it can confirm the presence of metal (Cu^{2+}, Mn^{2+}, Fe^{3+}, Zn^{2+}) in the metalloporphyrin composites, and it was found that loading of porphyrin molecules on to the titania surface did not significantly change the oxidation state and the coordination of the metals in MTCPPs. These results not only confirmed the metalloporphyrins on the TSI composites, but also supported the UV-vis absorption spectra results.

The magnetic properties of the CuTCPP-TSI were investigated in comparison to iron oxide nanoparticles using a vibrating sample magnetometer as magnetization curves in Fig. 7. Both of the materials showed superparamagnetic behavior at room temperature, as there was no coercivity observed. The saturation magnetization (Ms) of the iron oxide (I) nanoparticle was 58 emu/g corresponding to magnetite nanoparticles with excess oleic acid surfactant [18], whereas CuTCPP-TSI nanocomposites were 19 emu/g. After the coating process, the Ms values of the materials were obviously reduced, which was mainly due to the diamagnetic content in the nanocomposites.

The photocatalytic activity of the MTCPP-TSI that contained different metal centers was defined by measuring the photodegradation of methylene blue (MB) in aqueous solution under visible light irradiation. As shown in Fig. 8, the photodegradation of MB by TSI and MTCPP-TSI magnetic photocatalysts with different metal centers and free-metal on the porphyrin exhibited significant differences in the photocatalytic behaviors. The CuTCPP-TSI magnetic composites showed the best photocatalytic performance in that it could degrade 98% MB within 3 h of irradiation, while the photodegradation rate of MB by TSI was only 2.9% under the same condition. For the photodegradation rate of ZnTCPP-TSI, MnTCPP-TSI, FeTCPP-TSI, and TCPP-TSI were 58%, 36%, 29%, and 21%, respectively. All MTCPP-TSI nanocomposites exhibited enhanced photocatalytic activity compared to TSI nanocomposites. The degradation of MB was increasing in the order of CuTCPP-TSI > ZnTCPP-TSI > MnTCPP-TSI > FeTCPP-TSI > TCPP-TSI, which is in agreement with previous reports of photocatalytic results of metalloporphyrin anchored on titania [5], resulting from that metalloporphyrin anchored on titania particles can efficient generation of $O_2^{\cdot -}$.

However, we could observe a little difference in the absorbance of MTCPPs of different types, indicating that the dyes attached on TSI were of a little difference in weight ratio. To get rid of the effect from the quantity of the dyes and understand the effect of the type of metal centers on the photocatalytic activity, we calculated the percentage of dyes covering on TSI using the absorbance at λ_{max} of each dye subtracted with the background from TSI absorbance. When comparing the photocatalytic activity based on the same amount of porphyrin, the percentage of degradation methylene blue per percentage of porphyrin

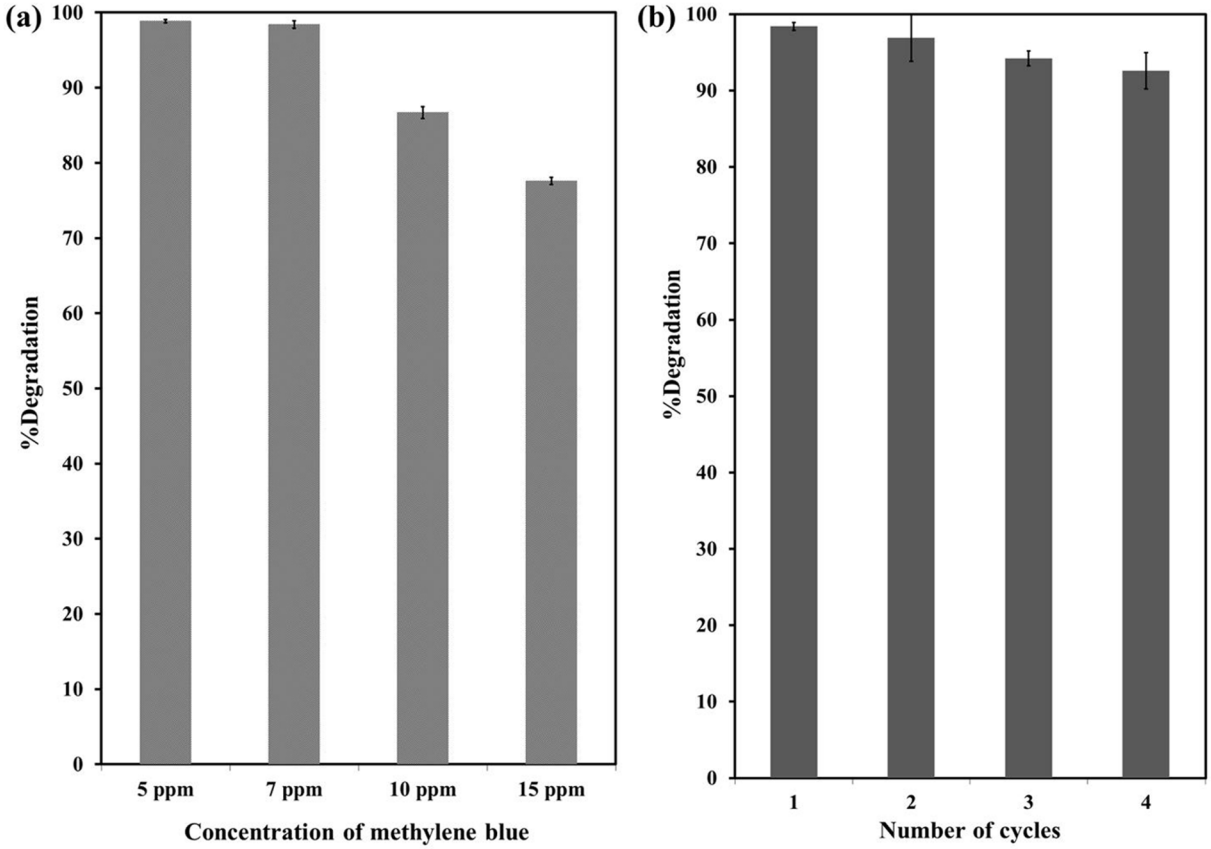

Fig. 9. The photodegradation of methylene blue upon visible light irradiation using CuTCPP-sensitized titania-silica-iron oxide nanocomposite (CuTCPP-TSI) (a) in different concentration of methylene blue, and (b) at different cycles of reused CuTCPP-TSI.

dye covered on TSI nanocomposites was calculated to 32%, 13%, 18%, 17% and 6% for CuTCPP-TSI, ZnTCPP-TSI, MnTCPP-TSI, FeTCPP-TSI, and TCPP-TSI, respectively. Among different metal porphyrins, the photodegradation increased in the following order: CuTCPP-TSI > MnTCPP-TSI, FeTCPP-TSI > ZnTCPP-TSI > TCPP-TSI based on the same amount of porphyrin on composites. These results indicated that metalloporphyrin containing a central metal ion with unfilled d orbitals showed higher photocatalytic activity when compared with the same amount of porphyrin dye. ZnTCPP-TSI with a filled d orbital has reached a stabilized condition, and thus it is difficult to accept or transfer external electron, leading to the low efficiency for photogenerated electrons and holes [6,19,20]. It has been discussed in previous study that CuTCPP exhibits short lifetime of excite state and forms the redox Cu(II)/Cu(I)/Cu(II) loop that is able to catch the generated electron from photoactivation. [21] These electrons can transfer to oxygen molecules, resulting in an increase in the radical species in the solution. The findings from MTCPP-TSI photocatalysts study suggested that the CuTCPP-TSI nanocomposites showed highest photocatalytic efficiency in the degradation of methylene blue under visible irradiation.

The effect of initial concentration of methylene blue on the photodegradation efficiency was studied using various methylene blue concentrations ranging from 5 to 15 ppm with a constant nanocomposite weight of 10 mg. Methylene blue solution is fixed at 30 mL for 3 h irradiation time. As a trend in Fig. 9a, the photodegradation efficiency decreased with an increase in methylene blue concentration. As the initial concentration of methylene blue increased, but constant nanomaterials were dispersed in MB solution, radicals generated from the composites were likely not enough to degrade MB at high concentration, resulting in the decrease in photodegradation efficiency. Moreover, at high concentration of methylene blue, the visible light penetrated less into methylene blue solution, resulting in reduction of the radicals formed. Thus, the photocatalytic activity decreased when increasing methylene blue concentration.

For the investigation of reusability of CuTCPP-TSI nanocomposites, after completing photocatalytic oxidation the catalysts were separated out of the reaction mixture by magnetic separation using an external magnetic field, and the composites were easily reused. The photodegradation was examined in each cycle of reused composites without regeneration process. As shown in Fig. 9b, only a small decrease in degradation rate was observed after four successive cycles. From these observation, the photocatalytic activity of the CuTCPP-TSI nanocomposites exhibited no significant decrease after several reaction cycles without regeneration of the catalyst. After four cycles, the CuTCPP-TSI nanocomposites still decomposed methylene blue with only a slight loss of photocatalytic activity because of the incomplete degradation in previous reaction that could lead to by-product deposition onto the composite surface. Diffuse reflectance UV-vis absorption spectra of the CuTCPP-TSI after used for four cycles (Fig. S3 in Supplementary) revealed that the Soret band of CuTCPP-TSI remained at around 415 nm similar to the fresh one, indicating that the CuTCPP was attached on the TSI with high stability for the photocatalysis reaction. Moreover, a new broad signal at around 662 nm could be the residues from methylene blue photodegradation that obscured the Q band of CuTCPP, supporting the rationale for the loss of photocatalytic activity of the nanocomposites.

Moreover, the nanocomposites were tested for the bactericidal activity using Gram negative pathogen *E. coli* as a testing model as previously described [12]. We hypothesized that irradiated CuTCPP-TSI nanocomposites produces reactive oxygen radicals, including superoxide anions and hydroxyl radicals that are highly toxic to bacteria cells causing oxidative damages to macromolecules such as nucleic acids,

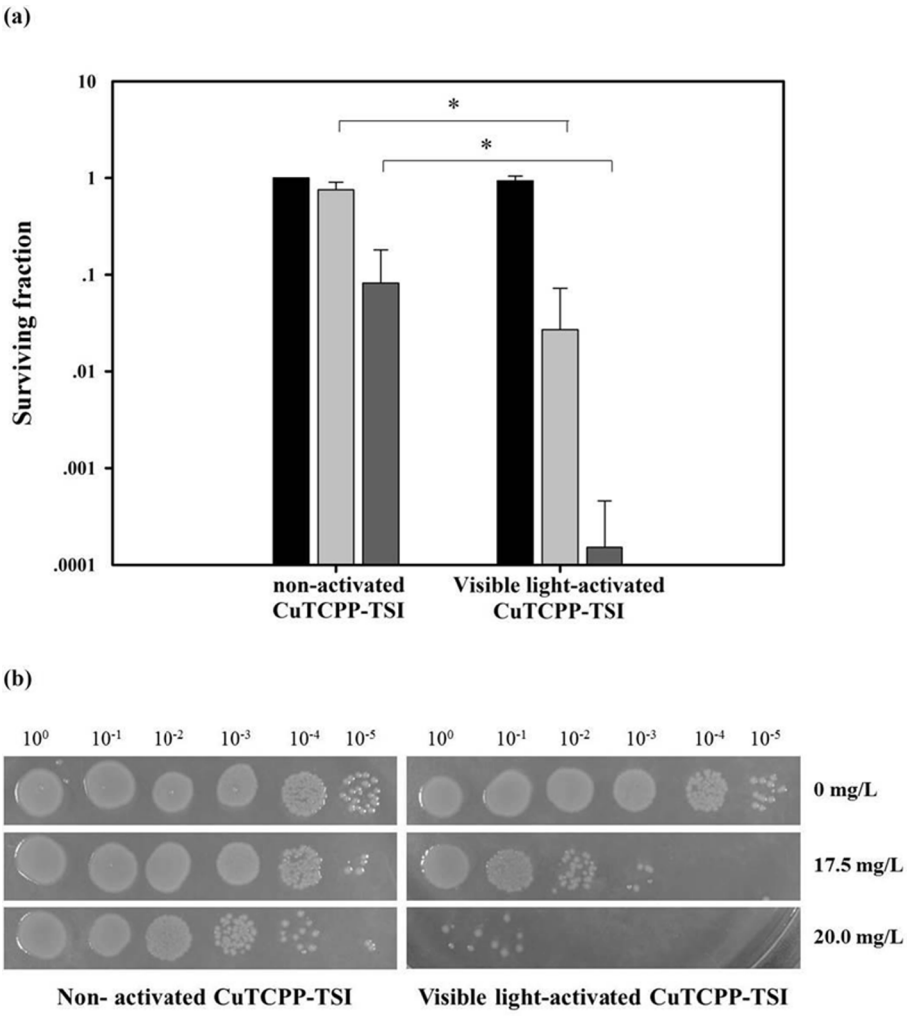

Fig. 10. The bactericidal activity of CuTCPP-TSI against *E. coli*. (a) The exponential cells were treated with non-activated and visible-light-activated CuTCPP-TSI nanocomposites at 0 mg/L (black bar), 17.5 mg/L (light gray bar) and 20.0 mg/L (dark gray bar) for 3 h then, the cells were 10-fold serial diluted and spotted on agar plate. The survival cells were counted after incubation at 37 °C for 24 h. The surviving fraction is defined as the number of colony forming units (CFU) of nanocomposites treated conditions divided by the untreated control. Data shown are mean SD of at least three independent experiments. The asterisk (*) indicated statistically different (p-value < 0.5, paired t-test). (b) The image of representative plate of nanocomposites-treated bacteria.

proteins, and membrane lipids, which can lead to bacterial cell death. This notion was supported by the ability of the light activated nanocomposites to degrade methylene blue (Fig. 9) because it has been reported that hydroxyl radical and superoxide anions are main species accounted for methylene blue degradation [22]. The exponential cells were treated with various concentrations of nanocomposites and activated with visible light, compared to non-activated nanocomposites. The results revealed that the visible light-activated CuTCPP-TSI nanocomposite could efficiently kill the bacteria. The 90% of the bacteria were killed by 17.5 mg/L of nanocomposites, whereas the bacteria were dramatically killed (99.9%) when the nanocomposite concentration was increased to 20.0 mg/L. This antibacterial activity was also concentration-dependent. In addition, the nanocomposite also possessed the bactericidal activity without visible light irradiation due to the nature of the nanocomposite, which made of the copper and titanium. These metals are known as the toxic substances for the bacteria. As the result shown in Fig. 10, only 20.0 mg/L of nanocomposites killed *E. coli* significantly. Thus, the bacterial killing activity is more effective upon activation of nanocomposites with visible light.

4. Conclusions

Tetra(4-carboxyphenyl)porphyrin with different metal centers [Mn (II), Fe(III), Cu(II), Zn(II)] loaded on the surface of titania-silica-iron oxide nanocomposites (TSI) has been successfully prepared and investigated for their photocatalytic activity by the degradation of methylene blue (MB) under visible light irradiation. Under this condition, the results showed that TSI sensitized by CuTCPP can efficiently degrade 98% of methylene blue solution due to enlargement of the wavelength response for utilization of sunlight energy. The four-cycled reuse of the CuTCPP-TSI results suggested the great reusability of the magnetic photocatalyst. Furthermore, these magnetic photocatalyst exhibited high antibacterial reactivity. Because CuTCPP-TSI nanocomposites exhibit magnetic responses and high photocatalytic activity, CuTCPP-TSI can possibly be used in organic pollutant degradation and the eradication of bacteria under magnetic control and separation. By using the visible light activated the nanocomposite will lead to the variety of the application without sophisticated equipment.

Acknowledgments

This work was financially supported by the Ratchadapiseksomphot Endowment Fund under the Outstanding Research Performance Program, Chulalongkorn University (Sci-Super III-003). Staff mobility was carried out with funding from Grant for Join Funding, Ratchadapiseksomphot Endowment Fund. P. Chanhom graduate study was financially supported by the 100th Anniversary Chulalongkorn University Fund for Doctoral Scholarship, Graduate School, Chulalongkorn University and the 90th Anniversary of Chulalongkorn University Fund. The authors would also like to thank the Synchrotron Light Research Institute for XPS measurement and Associate Professor Patchanita Thamyongkit and Dr. Paiboon Vattanaviboon for valuable discussion.

Appendix A. Supplementary data

Supplementary data to this article can be found online at https://doi.org/10.1016/j.jmmm.2018.11.090.

References

[1] J. Schneider, M. Matsuoka, M. Takeuchi, J. Zhang, Y. Horiuchi, M. Anpo, D.W. Bahnemann, Chem. Rev. 114 (2014) 9919–9986.
[2] M. Pelaez, N.T. Nolan, M.K. Seery, P. Falaras, A. Kontos, P.S. Dunlop, J.W. Hamilton, J.A. Byrne, K.O. Shea, M.H. Entezari, D.D. Dionysiou, Appl. Catal., B: Environ. 125 (2012) 331–349.
[3] L.-L. Li, E.W. Diau, Chem. Soc. Rev. 42 (2013) 291–304.
[4] B. Yao, C. Peng, W. Zhang, Q. Zhang, J. Niu, J. Zhao, Appl. Catal., B: Environ. 174–175 (2015) 77–84.
[5] G. Granados-Oliveros, E.A. Páez-Mozo, F.M. Ortega, M.T. Piccinonato, F.N. Silva, C.L.B. Guedes, E.D. Mauro, M.F. Costa, A.T. Ota, J. Mol. Catal. A: Chem. 339 (2011) 79–85.
[6] G. Granados-Oliveros, E.A. Páez-Mozo, F.M. Ortega, C. Ferronato, J.-M. Chovelon, Appl. Catal. B: Environ. 89 (2009) 448–454.
[7] K.P. Kuhn, I.F. Chaberny, K. Massholder, M. Stickler, V.W. Benz, H.G. Sonntag, L. Erdinger, Chemosphere 53 (2003) 71–77.
[8] K. Sunada, T. Watanabe, K. Hashimoto, J. Photochem. Photobiol. A: Chem. 156 (2003) 227–233.
[9] T.-D. Pham, B.-K. Lee, Appl. Surf. Sci. 296 (2014) 15–23.
[10] S. Zargari, R. Rahimi, A. Yousefi, RSC Adv. 6 (2016) 24218–24228.
[11] D. Beydoun, R. Amal, G. Low, S. McEvoy, J. Phys. Chem. 104 (2000) 4387–4396.
[12] P. Chanhom, N. Charoenlap, B. Tomapatanaget, N. Insin, J. Magn. Magn. Mater. 427 (2017) 54–59.
[13] J. Park, K. An, W. Hwang, J.G. Park, H.J. Noh, J.Y. Kim, J. Park, N. Hwang, T. Hyeon, Nat. Mater. 3 (2004) 891–895.
[14] R. Giovannetti, The Use of Spectrophotometry UV-Vis for the Study of Porphyrins, in: J. Uddin (Ed.), Macro to Nano Spectroscopy, InTech, Croatia, Europe, 2012.
[15] Zsolt Valicsek, O. Horváth, Microchem. J. 107 (2013) 47–62.
[16] R. Rahimi, M.M. Moghaddas, S. Zargari, J. Sol-Gel Sci. Technol. 65 (2013) 420–429.
[17] Y.-J. Yuan, J.-R. Tu, Z.-J. Ye, H.-W. Lu, Z.-G. Ji, B. Hu, Y.-H. Li, D.-P. Cao, Z.-T. Yu, Z.-G. Zou, Dyes Pigments 123 (2015) 285–292.
[18] H.L. Ding, Y.X. Zhang, S. Wang, J.M. Xu, S.C. Xu, G.H. Li, Chem. Mater. 24 (2012) 4572–4580.
[19] X. Zhao, X. Liu, M. Yu, C. Wang, J. Ji, Dyes Pigments 136 (2017) 648–656.
[20] S. Afzal, W.A. Daoud, S. Langford, Appl. Surf. Sci. 275 (2013) 36–42.
[21] N. MD, H.-B. R, G. M, J. Porphyr. Phthalocya. 3 (1999) 230–237.
[22] Z.M. Abou-gamra, M.A. Ahmed, J. Photochem. Photobiol. B 160 (2016) 134–141.